Title
LIMIT ON BOTTOM-HADRON PRODUCTION BY 209-GeV MUONS

Permalink
https://escholarship.org/uc/item/1xq4r5cj

Author
Clark, A.R.

Publication Date
1980-12-01

LBL-11543 c.2
Preprint

Lawrence Berkeley Laboratory
UNIVERSITY OF CALIFORNIA

Physics, Computer Science & Mathematics Division

Submitted to Physical Review Letters

LIMIT ON BOTTOM-HADRON PRODUCTION BY 209-GeV MUONS

A.R. Clark, K.J. Johnson, L.T. Kerth, S.C. Loken, T.W. Markiewicz, P.D. Meyers, W.H. Smith, M. Strovink, W.A. Wenzel, R.P. Johnson, C. Moore, M. Mugge, R.E. Shafer, G.D. Gollin, F.C. Shoemaker, and P. Surko

December 1980

LBL-11543 c.2

Prepared for the U.S. Department of Energy under Contract W-7405-ENG-48

LBL-11543

FERMILAB-Pub-80/81-exp

C00-3072-114

Limit on Bottom-Hadron Production by 209-GeV Muons

A.R. Clark, K.J. Johnson, L.T. Kerth, S.C. Loken, T.W. Markiewicz, P.D. Meyers, W.H. Smith, M. Strovink, and W.A. Wenzel

Physics Department and Lawrence Berkeley Laboratory
University of California, Berkeley, California 94720

R.P. Johnson, C. Moore, M. Mugge, and R.E. Shafer

Fermi National Accelerator Laboratory
Batavia, Illinois 60510

G.D. Gollin[a], F.C. Shoemaker, and P. Surko[b]

Joseph Henry Laboratories, Princeton University
Princeton, New Jersey 08544

Analysis of 36 952 dimuon final states produced by 209-GeV muons in a magnetized-iron calorimeter has been used to set the 90%-confidence level limit $\sigma(\mu N \to b\bar{b}X)B(b\bar{b} \to \mu X) < 2.9\times10^{-36}$ cm^2 for the production of bottom hadrons. Using B=0.17, the bound on the cross section for 160-GeV photons extrapolated to $Q^2=0$ is $\sigma(\gamma N \to b\bar{b}X) < 4.3$ nb. These limits conflict with several model calculations based on vector-meson dominance.

We report a limit on the muoproduction of hadrons containing bottom quarks. The limit is based on the analysis of 36 952 dimuon final states produced by 1.4×10^{11} positive and 2.9×10^{10} negative 209-GeV muons in the Berkeley-Fermilab-Princeton multimuon spectrometer at Fermilab.

We have calculated the expected rate for bottom meson production using a photon-gluon-fusion (γGF) model[1] which accounts for most of the published features[2] of charmed meson production. Using a distribution $g(x)=3(1-x)^5/x$ in gluon momentum fraction x, a bottom quark mass $m_b=4.7$ GeV/c^2 and charge $|q_b|=1/3$, and a strong coupling constant $\alpha_s=1.5/\ln(4m^2_{b\bar{b}})$, where $m_{b\bar{b}}$ is the mass of the produced quark pair, the model predicts a $b\bar{b}$ muoproduction cross section of 0.93×10^{-36} cm^2 at 209 GeV. If the $b\bar{b}\rightarrow\mu X$ branching ratio B is assumed to be 0.17 (essentially the same as that for $c\bar{c}\rightarrow\mu X$), the predicted σB is 0.16×10^{-36} cm^2.

The muon beam was incident on a solid steel dipole magnet composed of (91) 10-cm-thick plates interleaved with scintillation counters and wire chambers. The steel served as a target, hadron calorimeter, muon identifier, and momentum-analyzing muon spectrometer. The dimuon trigger and reconstruction algorithms have been described elsewhere[2,3]. Cuts were applied to reduce the contribution from π and K decay to (27±14)% of the dimuon sample. These cuts require a 9 GeV minimum daughter muon energy, a minimum ν of 75 GeV, a 0.2 GeV/c minimum daughter muon momentum, $p_\perp$, transverse to the virtual photon, and a range in inelasticity, $y=1-$(daughter muon energy)$/\nu$, of $0.675<y<0.95$. Histograms of simulated π- and K-decay events are subtracted bin by bin from the data histograms. Almost all of the remaining events are attributed to charmed meson decay. These events are simulated with a γGF model, using the Monte Carlo program described in Ref. 2. Background-subtracted data and charm Monte Carlo agree precisely in ν and adequately in

Q^2, y, and daughter muon energy, while $p_\perp$ is higher in the data by 15%[2].

Monte Carlo simulation of $b\bar{b}$ muoproduction is based on the γGF model described above. The b quarks are assumed to fragment into pairs of bottom mesons which decay to D mesons[4]. The fragmentation functions used are identical to those described in Ref. 2. Further muon-producing cascade decays are ignored, because they tend to produce decay muons which are indistinguishable from charm background. The simulated detection efficiency for $b\bar{b}$ states decaying directly to at least one muon is 19%.

The ratio of simulated bottom quark events to simulated charm quark events is highest in the region $\nu > 150$ GeV and $p_\perp > 1.4$ GeV/c. Hereafter we refer to this region as $R_{b\bar{b}}$. The intent of the $b\bar{b}$ analysis reported here is to reshape slightly the $c\bar{c}$ Monte Carlo distributions in Q^2, y, $p_\perp$, and ν in order to achieve full agreement with the data outside $R_{b\bar{b}}$. The empirically determined event-weighting functions which accomplish this reshaping then are extrapolated into $R_{b\bar{b}}$, and are used to reshape the $c\bar{c}$ Monte Carlo distributions within that region. The spectra inside $R_{b\bar{b}}$ of the reshaped charm Monte Carlo and the background-subtracted data finally are compared to search for a possible $b\bar{b}$ signal.

The charm Monte Carlo spectra are reshaped by weighting each simulated $c\bar{c}$ event by a product of three functions, respectively of Q^2, y, and (ν and $p_\perp$). The weighting functions were $(1+Q^2/70(\mathrm{GeV}/c)^2)^{-2}$, a polynomial[5] in y and the function of ν and $p_\perp$ listed in Table 1. The last function was determined by a two-dimensional fit in the ν-$p_\perp$ plane. Since Q^2 and y are only weakly correlated with $p_\perp$ and ν it was possible to determine the three weighting functions by iteration. After weighting by all three functions, each event was added to each histogram to produce the reshaped spectra. Before and after weighting, the charm Monte Carlo sample was normalized to the background-subtracted data outside $R_{b\bar{b}}$.

Figures 1 and 2 show background-subtracted data compared to the original and weighted $c\bar{c}$ Monte Carlo spectra in Q^2 and y. Also shown is 100× the $b\bar{b}$ signal (with $\sigma B=0.16\times10^{-36}$ cm^2) expected from the γGF model. These spectra are populated only by events outside of $R_{b\bar{b}}$. Figures 3 and 4 make the same data-$c\bar{c}$-$b\bar{b}$ comparison. Figure 3 displays the ν spectra for $p_\perp>1.4$ GeV/c and $p_\perp<1.4$ GeV/c, and Fig. 4 shows the $p_\perp$ spectra for ν>150 GeV and ν<150 GeV. These figures emphasize the consistency between data and reshaped charm Monte Carlo outside $R_{b\bar{b}}$. Specifically, in the ν-$p_\perp$ plane outside $R_{b\bar{b}}$ the χ^2 for a unit ratio of data to $c\bar{c}$ Monte Carlo is 190 for 176 degrees of freedom.

The region $R_{b\bar{b}}$ contains 3.4 simulated bb events, or 29.5% of the Monte Carlo $b\bar{b}$ sample, and 455 $c\bar{c}$ events, or only 1.5% of the weighted Monte Carlo $c\bar{c}$ sample. After subtraction of the four simulated π- and K-decay background events, 456 data events remain in $R_{b\bar{b}}$. The error in the difference between data and Monte Carlo is $(\sigma_1{}^2+\sigma_2{}^2+\sigma_3{}^2)^{\frac{1}{2}}$, where $\sigma_1=22$ is the random error in the number of background-subtracted data events in $R_{b\bar{b}}$ and $\sigma_2=37$ is the error in the number of $c\bar{c}$ Monte Carlo events in $R_{b\bar{b}}$. Included in σ_2 are the random error in the ratio of Monte Carlo to data outside $R_{b\bar{b}}$, the error in weighting cc Monte Carlo events within $R_{b\bar{b}}$ based on the spectra outside $R_{b\bar{b}}$, and the random error in the generated number of these events. The error analyses which determine σ_1 and σ_2 take fully into account the statistical effects of variations in the amount of subtracted background and in the weights assigned to individual events. The systematic error induced by uncertainty in π- and K-decay background, $\sigma_3=20$, is determined by repeating the entire analysis with the background multiplied by 0.5 or 1.5. The resulting $b\bar{b}$ signal is (1±48) events, corresponding to fewer than 62 candidates with 90% confidence.

To ensure that any $b\bar{b}$ events outside $R_{b\bar{b}}$ do not affect the number of expected

$c\bar{c}$ events in $R_{b\bar{b}}$, the analysis was repeated with 14× the simulated $b\bar{b}$ signal (corresponding to 48 events in $R_{b\bar{b}}$) added to the background-subtracted data. The simulated $c\bar{c}$ signal in $R_{b\bar{b}}$ changed by less than one event.

With our luminosity and calculated detection efficiency, the <62 candidates produce the 90%-confidence limit $\sigma(\mu N \to b\bar{b}X)B(b\bar{b} \to \mu X) < 2.9 \times 10^{-36}$ cm^2. Using B=0.17, $\sigma(\mu N \to b\bar{b}X) < 17 \times 10^{-36}$ cm^2. After factoring out the equivalent flux[6] of transversely polarized virtual photons, the muoproduction limit restricts $\sigma(\gamma N \to b\bar{b}X) < 4.3$ nb at an average virtual photon energy of 160 GeV, when the same branching ratio assumption is made.

Our limits are greater than some published predictions using γGF calculations, but conflict with others and with several vector meson dominance (VMD) models. The γGF calculations in Refs. 1 and 7 predicted $\sigma(\mu N \to b\bar{b}X) = 1\text{-}3 \times 10^{-36}$ cm^2 and 4×10^{-36} cm^2, respectively. Ref. 8 used a γGF model to derive $\sigma(\gamma N \to b\bar{b}X) = 16$ nb at 160 GeV. The authors of Ref. 9 employed a γGF approach with a fixed strong coupling constant to get $\sigma(\gamma N \to b\bar{b}X) = 0.2$ nb. They also obtained $\sigma(\gamma N \to b\bar{b}X) = 0.02\text{-}0.05$ nb with calculations using a running coupling constant with various gluon momentum distributions, but found 22 nb using VMD-based calculations. The VMD-model calculation of Ref. 10 yielded $\sigma(\gamma N \to b\bar{b}X) = 25$ nb; Ref. 11 predicted $\mathcal{O}(1\text{-}10$ nb) on the basis of empirical formulae and a sum rule derived by Shifman et al.[12]. The generalized VMD calculation in Ref. 13 found that the $b\bar{b}$ photoproduction cross section could be as high as 125 nb.

We are grateful for the dedicated efforts of many individuals at our respective institutions. We thank particularly the staffs of the Lawrence Berkeley Laboratory and Fermilab computer centers. This work was supported by the High Energy Physics Division of the U.S. Department of Energy under Contract Nos. W-7405-Eng-48, DE-AC02-76ER03072, and EY-76-C-02-3000.

References

[a]Now at Enrico Fermi Institute, Chicago, IL 60637.

[b]Now at Bell Laboratories, Murray Hill, NJ 07974.

[1]J.P. Leveille and T. Weiler, Nucl. Phys. B147, 147 (1979), and references cited therein.

[2]A.R. Clark et al., Phys. Rev. Lett. 45, 682 (1980).

[3]A.R. Clark et al., Phys. Rev. Lett. 43, 187 (1979).

[4]We use the decay matrix elements of I. Hinchliffe and C.H. Llewellyn Smith, Nucl. Phys. B114, 45 (1976).

[5]The polynomial is $1.0-7.56y+19.81y^2-21.79y^3+8.66y^4$.

[6]F.J. Gilman, Phys. Rev. 167, 1365 (1968).

[7]V. Barger, W.Y. Keung, and R.J.N. Phillips, Phys. Rev. D20, 630 (1979).

[8]H. Fritzsch and K.H. Streng, Phys. Lett. 72B, 385 (1978).

[9]J. Babcock, D. Sivers, and S. Wolfram, Phys. Rev. D18, 162 (1978).

[10]D. Horn, Phys. Lett. 73B, 199 (1978).

[11]J. Ellis et al., Nucl. Phys. B131, 285 (1977).

[12]M.A. Shifman, A.I. Vainshtein, and V.I. Zakharov, Phys. Lett. 65B, 255 (1978).

[13]B. Margolis, Phys. Rev. D17, 1310 (1978).

TABLE 1. Weighting function $R(\nu,p_\perp)$ for daughter muon momentum, $p_\perp$, transverse to the virtual photon and beam muon energy loss ν.

$f = \log_{10}(p_\perp)$

$R(\nu,f) = P(\nu,f)\cdot F(f)$

$P(\nu,f) = 1.43+a_0\nu+b_0 f+c_0\nu\cdot f+d_0\nu^2+e_0 f^2$

$F(f) = (L_1(f)+L_2(f))/(L_3(f)+L_4(f))$

$L_i(f) = (a_i+b_i f)/(|c_i-f|^{d_i}+e_i)\ (1\leq i\leq 4)$

i	a_i	b_i	c_i	d_i	e_i
0	-.0022	-.086	-.0021	-9.3×10^{-6}	-.57
1	181	165	-.17	2.1	0.04
2	-.032	0.031	0.29	5.7	$2.8\ 10^{-5}$
3	44	3.9	-.20	2.6	0.010
4	-.0045	0.0074	0.30	6.4	9.8×10^{-6}

Figure Captions

FIG. 1. Original and weighted $c\bar{c}$ Monte Carlo Q^2 spectra, compared with data after subtraction of the simulated π- and K-decay background. All events lie outside of $R_{b\bar{b}}$, the region where $\nu>150$ GeV and the momentum, $p_\perp$, of the daughter muon transverse to the virtual photon exceeds 1.4 GeV/c. Also shown is the simulated Q^2 spectrum for 100× the $b\bar{b}$ signal expected from the γGF model.

FIG. 2. Original and weighted $c\bar{c}$ Monte Carlo inelasticity $y=1-$(daughter muon energy)/ν, compared with background subtracted data, for events lying outside of $R_{b\bar{b}}$. Also shown is the simulated y spectrum for 100× the $b\bar{b}$ signal expected from the γGF model.

FIG. 3. Original and weighted $c\bar{c}$ Monte Carlo ν spectra, compared with background subtracted data for (a) $p_\perp>1.4$ GeV/c and (b) $p_\perp<1.4$ GeV/c. Also shown are the simulated ν spectra for 100× the $b\bar{b}$ signal expected from the γGF model.

FIG. 4. Original and weighted $c\bar{c}$ Monte Carlo $p_\perp$ spectra, compared with spectra of background subtracted data for (a) $\nu>150$ GeV and (b) $\nu<150$ GeV. Also shown are the simulated $p_\perp$ spectra for 100× the $b\bar{b}$ signal expected from the γGF model.

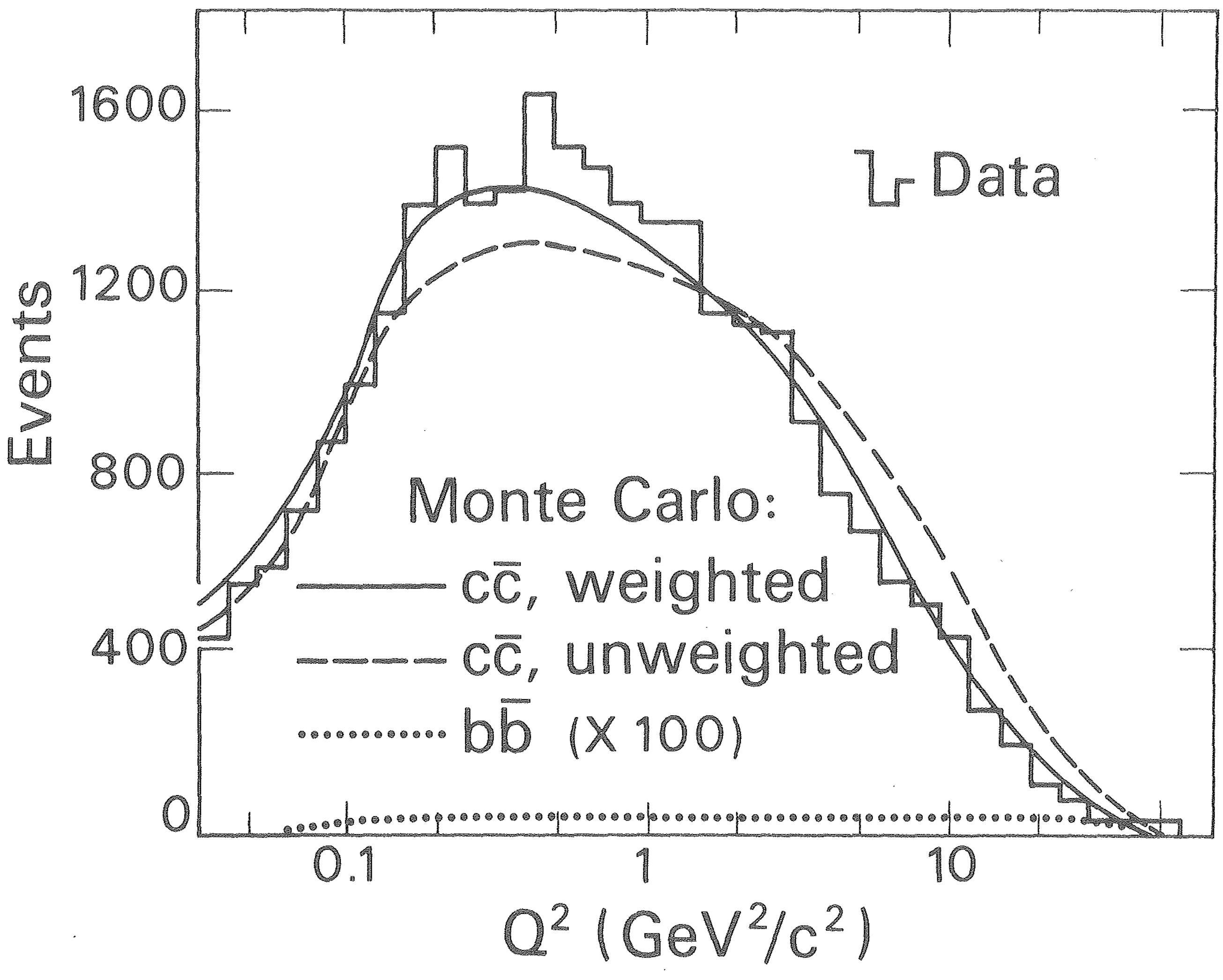

XBL 8011-2411

FIG. 1

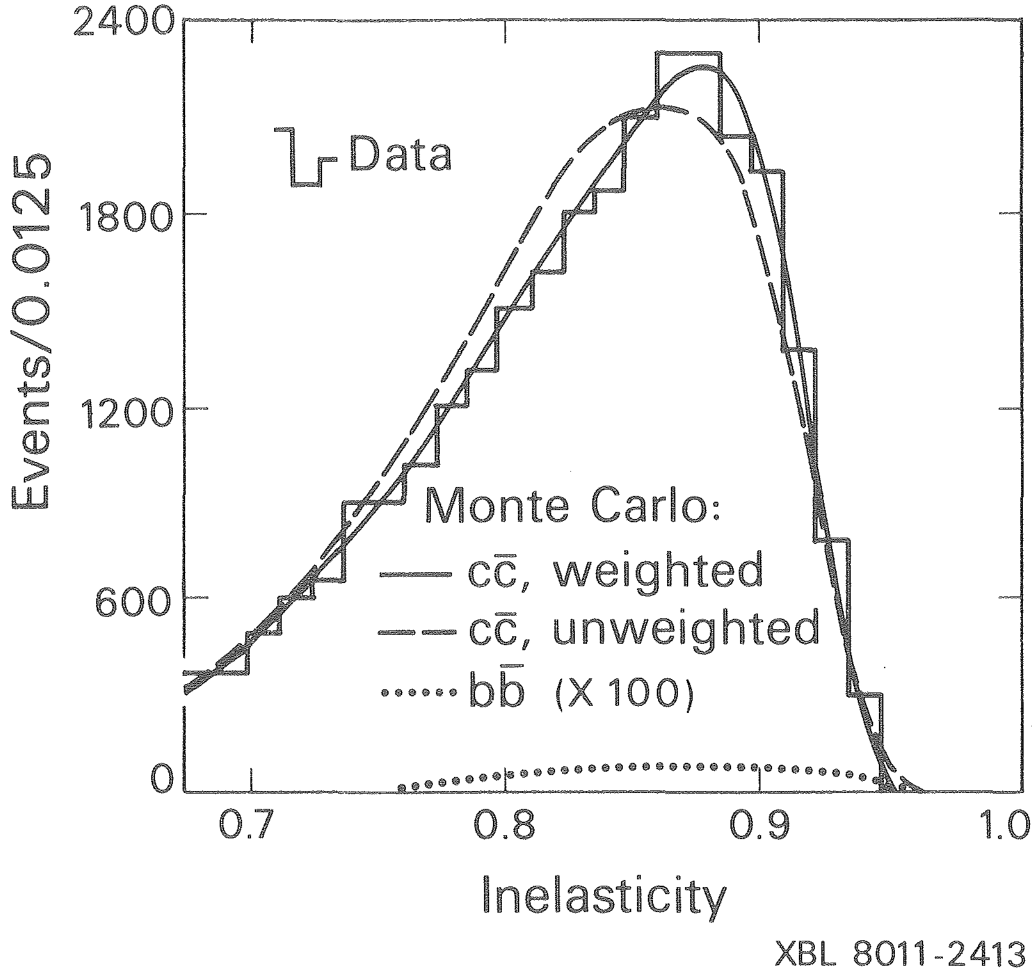
2400
1800
1200
600
0
Events/0.0125
Data
Monte Carlo:
cc̄, weighted
cc̄, unweighted
bb̄ (X 100)
0.7
0.8
0.9
1.0
Inelasticity
XBL 8011-2413

FIG. 2

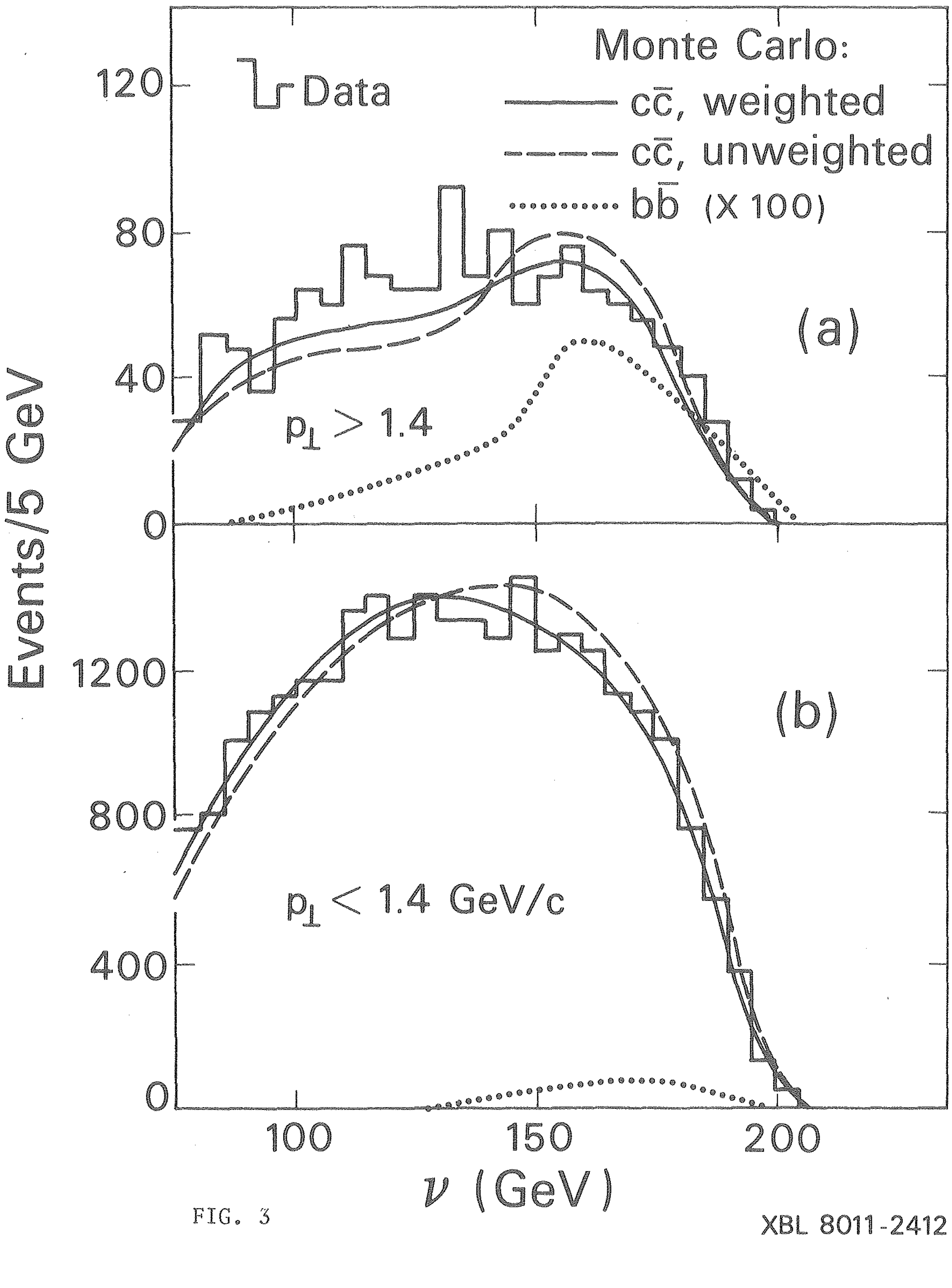

FIG. 3

XBL 8011-2412

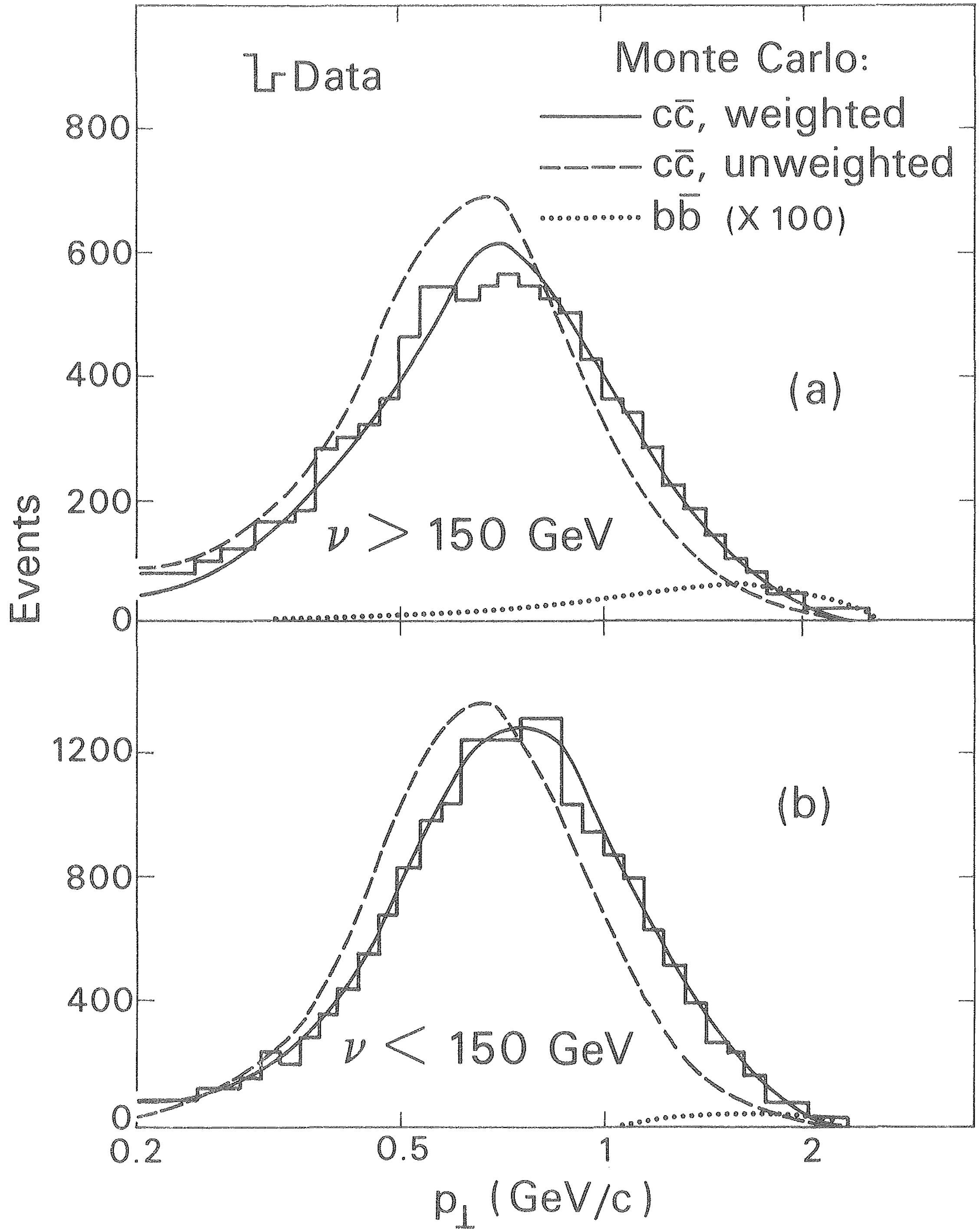

FIG. 4

XBL 8011-2410